Mixing characteristics and structure of a turbulent jet diffusion flame stabilized on a bluff-body

By S. H. Kim AND H. Pitsch

1. Motivation and objectives

A bluff-body stabilized jet diffusion flame is an interesting model problem with relevance to many engineering combustion systems (Masri & Bilger 1984; Dally *et al.* 1998). In the Sydney bluff-body flame configuration, which has been a standard target flame in the turbulent combustion community, the central fuel jet is surrounded by a bluff-body and is injected at high velocity, while the coflow air stream enters on the outside of the bluff-body. As in backward facing step and bluff-body wakes, vortex shedding occurs, and large scale recirculating flows are generated in the bluff-body stabilized flame. The complex recirculating flows are known to help flame stabilization by entraining hot combustion products into upstream locations. However, details of flow dynamics, scalar mixing and flame stabilization in the Sydney bluff-body configuration have not been fully understood yet.

Prediction of pollutants such as NO_x and soot is of both fundamental and practical interest. For accurate prediction of pollutants, a combustion model needs to consider the history of flame elements. Pollutant formation in a bluff-body stabilized flame has been predicted using the conditional moment closure (CMC) (Kim & Huh 2002) and the transported probability density function (PDF) method in Reynolds averaged Navier Stokes simulations (RANS) (Liu *et al.* 2005). In a first-order CMC prediction of a flame with low levels of local extinction, the major and stable intermediate species including CO are well predicted, while OH and NO are over-predicted (Kim & Huh 2002). Liu *et al.* (2005) applied the transported PDF model to the bluff-body stabilized flames with varying degrees of local extinction, HM1, HM2 and HM3. The calculations of HM2 and HM3, which have more significant extinction than HM1, do not reproduce the levels of local extinction observed in the experiment. This deficiency was attributed to inaccurate prediction of the mean mixture fraction in the recirculation zone. Their results also showed similar over-prediction of NO to that in Kim & Huh (2002).

Recently, Kim & Pitsch (2005) proposed the conditional filtering method as a subfilter model for nonpremixed combustion. It is an extension of CMC for LES and adopts filtering of the reactive scalar fields conditioned on the iso-surfaces of the mixture fraction, which allows small scale mixing and chemical reactions to be resolved in mixture fraction space (Kim & Pitsch 2005; Navarro-Martinez *et al.* 2005). Due to resolved large scale fluctuations of reactive scalars on the isopleth, closures of scalar fluxes in mixture fraction space and of chemical reaction source terms, which are of primary importance in a CMC-based method, were shown to be much improved as compared with those in the RANS framework. An integrated formulation was also proposed to reduce the computational cost (Kim & Pitsch 2005).

In this paper, the structure of turbulent jet diffusion flames stabilized on a bluff-body is investigated using large-eddy simulation (LES). Of particular interest are flow dynamics and the resulting influence on scalar mixing and flame structure. Pollutant predictions

in combustion LES of complex recirculating flows is also of interest. The conditional filtering method is used to describe sub-filter combustion processes and pollutant formation. An integrated formulation that considers only axial variation of conditionally filtered quantities is presented. Results are validated against experimental data of Dally et al. (1998).

2. Mathematical models

The spatially filtered equations for low Mach number variable density flows are solved in conjunction with dynamic models for subfilter quantities (Moin *et al.* 1991; Lilley 1992). The subfilter combustion processes are modeled by the conditional filtering method described below. The filtered density is obtained by

$$\frac{1}{\overline{\rho}} = \int_0^1 \frac{1}{\rho_\eta} \widetilde{P}_\xi(\eta) d\eta, \tag{2.1}$$

where ρ_η is the conditionally filtered density. ρ_η is obtained from the solution of the conditionally filtered equations for reactive scalars. $\widetilde{P}_\xi$ is the density-weighted filtered density function (FDF). Here $\widetilde{P}_\xi$ is assumed to be a beta distribution parameterized by the filtered mean and subfilter variance of the mixture fraction ξ. A dynamic approach is used to obtain the subfilter variance (Pierce & Moin 1998).

In the cylindrical coordinate, an integrated conditional filtering (Kim & Pitsch 2005) can be defined as

$$\overline{\phi|\eta}^*(\eta, x, t) \equiv \frac{\int_0^{2\pi}\int_0^\infty r \int_V \phi(\mathbf{x}, t)\delta(\xi(\mathbf{x}, t) - \eta) G(\mathbf{x} - \mathbf{x}'; \Delta_f) d\mathbf{x}' dr d\theta}{\int_0^{2\pi}\int_0^\infty r \int_V \delta(\xi(\mathbf{x}, t) - \eta) G(\mathbf{x} - \mathbf{x}'; \Delta_f) d\mathbf{x}' dr d\theta}, \tag{2.2}$$

where δ is the Dirac delta function and η is the sample space variable of the mixture fraction ξ. r and θ represent the radial and azimuthal coordinates, respectively. x is the axial coordinate. The integration is taken over the constant x plane in (2.2). The conditionally filtered quantity then has one independent variable that represents the spatial dependence. The one spatial coordinate x, together with the mixture fraction coordinate η, represents the history of flame elements.

The equation for the conditionally filtered mass fraction of species i, $\overline{Y_i|\eta}^*$, can be written as

$$\frac{\partial \overline{Y_i|\eta}^*}{\partial t} + \overline{U|\eta}^* \cdot \frac{\partial \overline{Y_i|\eta}^*}{\partial x} = \overline{N|\eta}^* \frac{\partial^2 \overline{Y_i|\eta}^*}{\partial \eta^2} + \overline{\omega_i|\eta}^* + F_i^* + \frac{\partial}{\partial x}\left(D_\eta^* \frac{\partial \overline{Y_i|\eta}^*}{\partial x}\right), \tag{2.3}$$

where

$$F_i^* = \frac{1}{\rho_\eta^* P_\xi^*} \frac{\partial}{\partial x}\left[\rho_\eta^* P_\xi^* \left(-\overline{UY_i|\eta}^* + \overline{U|\eta}^* \overline{Y_i|\eta}^*\right)\right]. \tag{2.4}$$

The superscript $*$ represents the integrated quantity. U is the axial velocity component. ρ_η is the conditionally filtered density. The conditional subfilter transport term F_i^* is modeled using the eddy diffusivity model:

$$F_i^* = \frac{\partial}{\partial x}\left(D_{t,\eta}^* \frac{\partial \overline{Y_i|\eta}^*}{\partial x}\right), \tag{2.5}$$

where

$$D^*_{t,\eta} = \frac{\int_0^{2\pi}\int_0^{\infty} \rho_\eta P_\xi D_t r dr d\theta}{\int_0^{2\pi}\int_0^{\infty} \rho_\eta P_\xi r dr d\theta}. \tag{2.6}$$

The terms involving the spatial derivative of $\rho^*_\eta P^*_\xi$ are assumed to be negligible in (2.5). (2.3) has the same form as the Eulerian laminar flame model, except for the subfilter transport term and the molecular diffusion term (Pitsch 2002).

In turbulent nonpremixed flames with little local extinction, fluctuations of reactive scalars are primarily associated with those of the mixture fraction. Fluctuations of reactive scalars on iso-η surfaces are then much smaller than those in $\mathbf{x}$ space. In first-order closure, the conditionally filtered reaction rate can be calculated as

$$\overline{\omega_i(\rho, \mathbf{Y}, T)|\eta}^* \approx \omega_i(\rho^*_\eta, \overline{\mathbf{Y}|\eta}^*, \overline{T|\eta}^*). \tag{2.7}$$

The conditionally filtered scalar dissipation rate is modeled by

$$\overline{N|\eta}^* = \frac{\int_0^{2\pi}\int_0^{\infty} \rho_\eta P_\xi N_0 \exp[-2(\mathrm{erf}^{-1}(2\eta-1))^2] r dr d\theta}{\int_0^{2\pi}\int_0^{\infty} \rho_\eta P_\xi r dr d\theta}, \tag{2.8}$$

where

$$N_0 = \frac{\widetilde{N}}{\int_0^1 \exp[-2(\mathrm{erf}^{-1}(2\eta-1))^2] d\eta}. \tag{2.9}$$

The functional form in the integral is obtained by the amplitude mapping closure (O'Brien & Jiang 1991). Following Girimaji & Zhow (1996), the filtered scalar dissipation rate $\widetilde{N}$ is modeled by

$$\widetilde{N} = (\widetilde{D} + D_t)\frac{\partial\widetilde{\xi}}{\partial x_i}\frac{\partial\widetilde{\xi}}{\partial x_i}, \tag{2.10}$$

where D is the molecular diffusivity of the mixture fraction. This corresponds to a local equilibrium assumption in which the production of the subfilter fluctuations of the mixture fraction is balanced with the dissipation term (Pierce & Moin 1998).

The conditionally filtered velocity is modeled by

$$\overline{U|\eta}^* = \frac{\int_0^{2\pi}\int_0^{\infty} \rho_\eta P_\xi \widetilde{U} r dr d\theta}{\int_0^{2\pi}\int_0^{\infty} \rho_\eta P_\xi r dr d\theta}, \tag{2.11}$$

where $\widetilde{U}$ is the axial component of the filtered velocity.

The density weighted filtered value of ϕ can be calculated by integration in η space:

$$\widetilde{\phi} = \frac{\int_0^1 \rho_\eta \overline{\phi|\eta}^* \widetilde{P}_\xi(\eta) d\eta}{\overline{\rho}}. \tag{2.12}$$

3. Numerical simulation

The present model is applied to turbulent jet diffusion flames stabilized on a bluff-body. The diameter of the bluff-body D_B is 50 mm, while that of the fuel jet is 3.6 mm. Fuel is composed of CH_4 and H_2 with a volumetric ratio equal to unity. The stoichiometric mixture fraction is equal to 0.05. Scalar statistics are taken with the fuel jet velocity of 118 m/s and the coflow air velocity of 40 m/s. The Reynolds number based on the fuel jet velocity and the diameter of the fuel jet nozzle is 15,800. Details on the experiments can be found in Dally *et al.* (1998a).

The filtered transport equations for low Mach number variable density flows are integrated by a structured finite volume solver, which is based on a energy conserving scheme and a semi-implicit iterative time integration (Pierce 1998). A second-order central differencing scheme is used for the spatial discretization of the velocity, while the BQUICK scheme is used for the mixture fraction to avoid significant wiggling (Pierce 1998; Herrmann *et al.* 2004). $256 \times 152 \times 64$ control volumes are used to resolve the large scale flow and mixing fields in a domain of $5.5D_B \times 1.5D_B \times 2\pi$. The present grid is based on that of Raman & Pitsch (2005), in which a grid refinement procedure for LES is presented by arguing that most scalar energy needs to be resolved for combustion LES. The present resolution for the radial and circumferential directions is essentially the same as that of Raman & Pitsch (2005), while the axial direction is better resolved. Inflow conditions are generated using a separate inflow generation code (Pierce 1998).

The equations for the conditionally filtered reactive scalars are solved using a stiff ordinary differential equation solver, VODE (Brown *et al.* 1989). Chemical reactions and diffusion in mixture fraction space are treated implicitly, while spatial transport terms are treated explicitly. The augmented reduced mechanism of Sung *et al.* (2001) is used to describe combustion and NO formation reactions. This reduced mechanism consists of 15 reaction steps involving 19 species and has been successfully used in simulations of piloted jet diffusion flames (Tang *et al.* 2000). The mixture fraction space is discretized by 75 grid points, while 64 grid points are used in the axial spatial coordinate. The molecular transport coefficients are obtained using the CHEMKIN package (Kee *et al.* 1996). Radiative heat loss is considered by the optically thin gray gas model.

The inlet conditions of the conditionally filtered quantities are available only at $\eta = 0$ and 1, i.e. for pure fuel and oxidizer. For the intermediate range of the mixture fraction, $0 < \eta < 1$, the inlet boundary condition is not physically meaningful, since there is no mixture with $0 < \eta < 1$ at the inlet. The commonly used inlet conditions, such as fully burning state close to chemical equilibrium or pure adiabatic mixing between fuel and oxidant, can result in unphysical influence on the solutions (Sreedhara & Huh 2005). To remedy this problem, we propose the following inlet boundary condition:

$$\begin{aligned} Q_i &= Y_{i,O} \quad \text{for } \eta = 0 \\ Q_i &= Y_{i,F} \quad \text{for } \eta = 1 \\ \frac{\partial Q_i}{\partial x}|_{x=0} &= 0 \quad \text{for } 0 < \eta < 1, \end{aligned}$$

where $Y_{i,O}$ and $Y_{i,F}$ are the mass fraction of species i in the oxidant and fuel streams, respectively. For the present case, the condition for $0 < \eta < 1$ is determined by the interaction with the wall, on which it is assumed that there are no scalar and heat fluxes. This boundary condition problem does not arise for the fully conservative formulation (Klimenko & Bilger 1999; Kim & Pitsch 2005).

4. Results and discussion

4.1. *Flow dynamics and scalar mixing*

Figure 1 shows the instantaneous fields of the filtered mixture fraction and scalar dissipation rate. At $x/D_B < 1.5$, the mixture is relatively well-mixed and the scalar dissipation rate is very low in the recirculation zone. The structures of the mixture fraction and the scalar dissipation fields near the centerline are similar to those in a simple jet flame at $x/D_B < 1$. The mixture fraction field indicates that shedding processes occur at

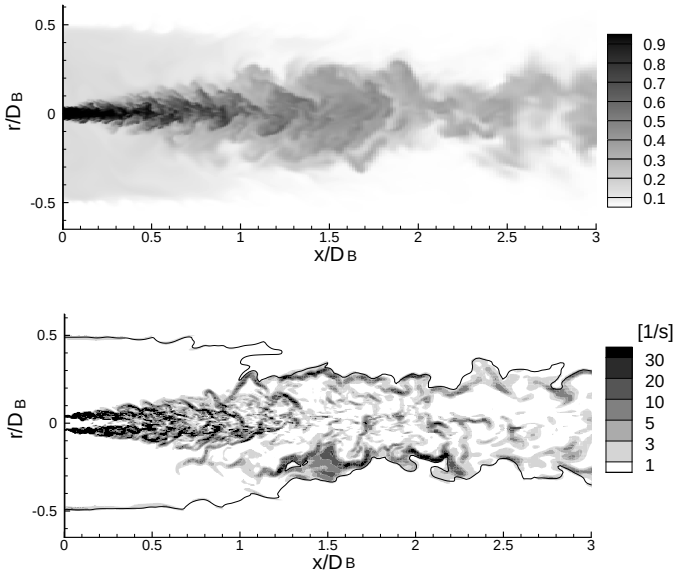

FIGURE 1. Instantaneous fields for the mixture fraction (top) and the scalar dissipation rate (bottom) at t=0.87 ms (the lines represent the stoichiometric surfaces).

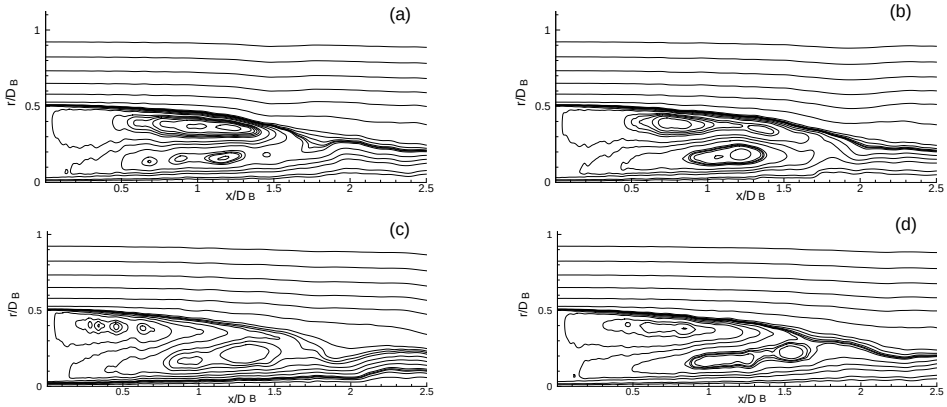

FIGURE 2. Streamlines for the azimuthally averaged velocity field (a) t=0 ms (b) t=0.87 ms (c) t=2.5 ms (d) t=3.3 ms.

downstream locations. The scalar dissipation rate on iso-surfaces of the stoichiometric mixture fraction, which is high near the bluff-body, decreases with axial distance in the recirculation zone. Note that the highest scalar dissipation rate on the iso-surfaces of the stoichiometric mixture fraction occurs at the end of the recirculation zone. High scalar dissipation rates are associated with the sheet-like structures, the length of which is comparable to that of large scale wrinkling of the stoichiometric surface in Fig. 1. The high dissipation layers are observed mostly at $r/D_B \approx 0.3$.

Figures 2(a)-(d) show streamlines for the azimuthally averaged velocity fields at several time instants. The velocity field has two large scale counter-rotating flow patterns, both of which consist of large scale eddies. The eddies in the inner recirculating pattern

contributes to spread the fuel mixture in the main jet more rapidly than in a simple jet, while those in the outer one entrain air from the coflow stream. The mixtures from the main jet and from the air coflow stream mix, while they are convected toward the bluff-body. Nearly uniform mixture composition is reached near the bluff-body due to the enhanced mixing. Note the oscillating behavior of the recirculating flow patterns in Figs. 2(a)-(d). In Fig. 2(a), the inner recirculating region is relatively short. The inner eddies then move to the downstream location and interact with the outer ones in Fig. 2(b). In Fig. 2(c), the outer eddies move back to the bluff-body, while the inner ones move toward the downstream location. After the backward movement, the outer eddies again move toward the downstream location in Fig. 2(d).

Figures 3(a)-(d) show the normalized total mixture fraction flux and the conditional scalar dissipation rates at several time instants. The normalized total mixture fraction flux is calculated by

$$\dot{m} = \frac{\int\int \overline{\rho}\widetilde{U}\widetilde{\xi} r dr d\theta}{\int\int \overline{\rho}_{in}\widetilde{U}_{in}\widetilde{\xi}_{in} r dr d\theta}, \tag{4.1}$$

where the subscript in denotes the inlet value. Fluctuations of $\dot{m}$ at $x/D_B \ll 1$ are associated with the dynamics of the main jet. The length scale over which $\dot{m}$ varies is small near the jet exit and increases with the axial distance. Note the sudden increase of this length scale at $1.2 < x/D_B < 2$ in Fig. 3(b). This abrupt increase of the length scale is associated with entrainment of air by vortex bubbles near the coflow stream, and interactions with the main jet. In Fig. 3(b), nearly equally spaced large scale structures are observed at $2 < x/D_B < 3$. The structures of the mixture fraction field in Fig. 1 are well characterized by the total mixture fraction flux, $\dot{m}$. Note that the occurrence of large scale structures at $1.2 < x/D_B < 2$ is associated with high scalar dissipation rates in Fig. 3. The scalar dissipation rate conditioned on $0.03 < \widetilde{\xi} < 0.08$, which represents the average scalar dissipation rate in the reaction zone, has a maximum at $x/D_B \approx 1.6$, which corresponds to the location of the minimum of $\dot{m}$. A similar behavior is observed for the scalar dissipation rate conditioned on $0.02 < \widetilde{\xi}$, which excludes only very small mixture fraction in the coflow air stream. In Fig. 3(c), the appearance of large scale structure of $\dot{m}$ is observed at $x/D_B \approx 0.7$, which is closer to the bluff-body than that in other time instants. This is because of the oscillation of large scale vortex bubbles. The outer recirculation bubble is located close to the bluff-body at this time, as shown in Fig. 2(c).

Figure 4(a) shows the velocity and scalar dissipation fields at $t = 0$ ms. There are two vortices, A and B, generated from the coflow air stream in Fig. 4(a). Note the high scalar dissipation rate near the vortex A. The high scalar dissipation layer is generated near the stagnation point, which is generated by the vortex A and the main jet. In this region, the main jet streams, which tend to flow outwardly at the end of the recirculation, collide with slowly moving outer vortices. Similar high dissipation layers are also observed near the vortex B. In Fig. 4(b), four vortices C-F are identifiable. The distance between two adjacent vortices is approximately $0.5D_B$. High dissipation layers are generated between two adjacent vortices. High dissipation layers at $1.2 < x/D_B < 2$ are oriented almost parallel to the flow direction. Large scale wrinkling of the dissipation layers is also observed. In Fig. 4(d), high scalar dissipation layers are also generated near the tip of the expanding main jet.

One of the motivations for a study of the bluff-body stabilized flame was the desire to generate a flame data base with intense mixing occurring in fully developed turbulence

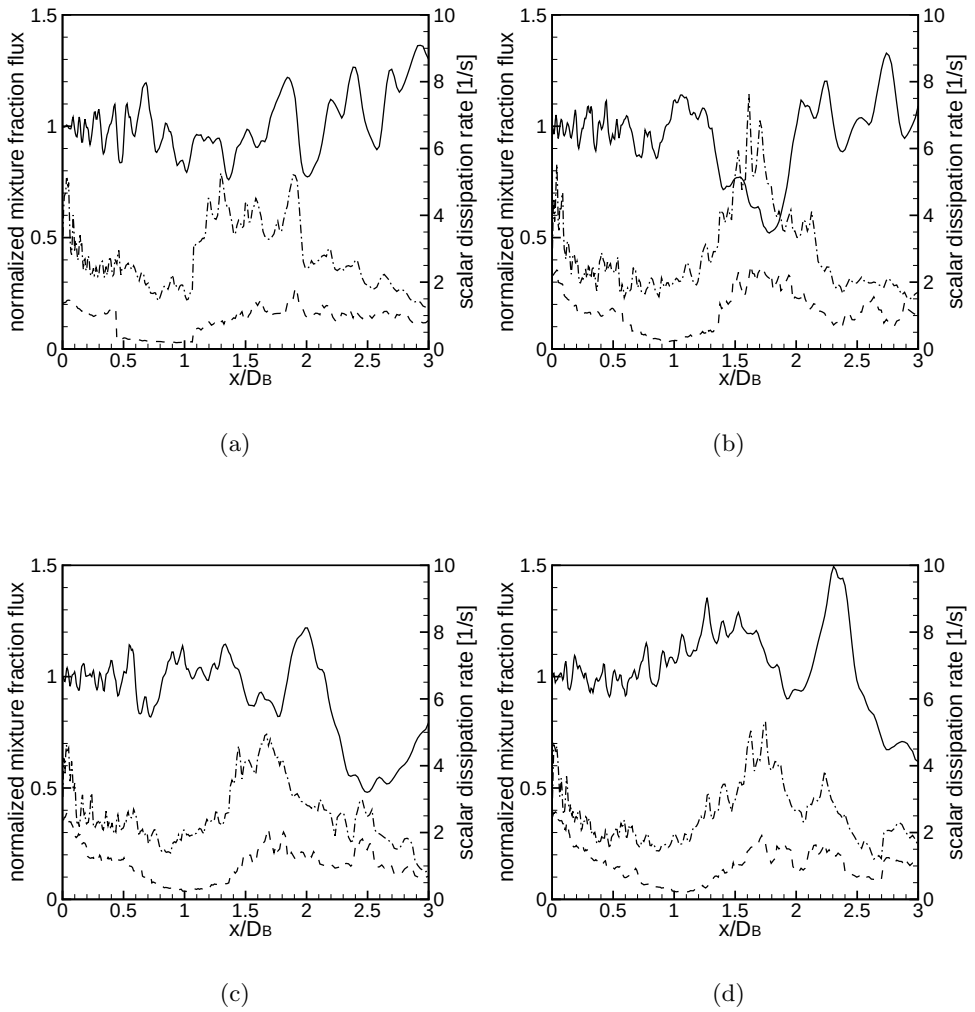

FIGURE 3. Axial distributions of the normalized total mixture fraction flux and the conditional scalar dissipation rates (a) t=0 ms (b) t=0.87 ms (c) t=2.5 ms (d) t=3.3 ms (solid line: normalized total mixture fraction flux, dashed line: average scalar dissipation rate conditioned on $0.03 < \widetilde{\xi} < 0.08$, dashed dotted line: average scalar dissipation rate conditioned on $0.02 < \widetilde{\xi}$).

away from the nozzle exit (Masri & Bilger 1984). The present results indicate that the intense mixing of fuel and air occurs at the end of the recirculation zone, in which turbulence is fully developed. At the end of the recirculation zone, $x/D_B \approx 1.6$, the fuel delivered by the main jet directly mixes with the air entrained by vortex bubbles in the coflow air stream. The complex interaction between the outer vortex bubbles and the high speed main jet makes intense mixing occur at the end of the recirculation zone. The flow dynamics in this intense mixing region is complicated and is strongly influenced by the vortex shedding mechanism.

The shedding of large scale vortical structures is typically observed in cylinder wakes,

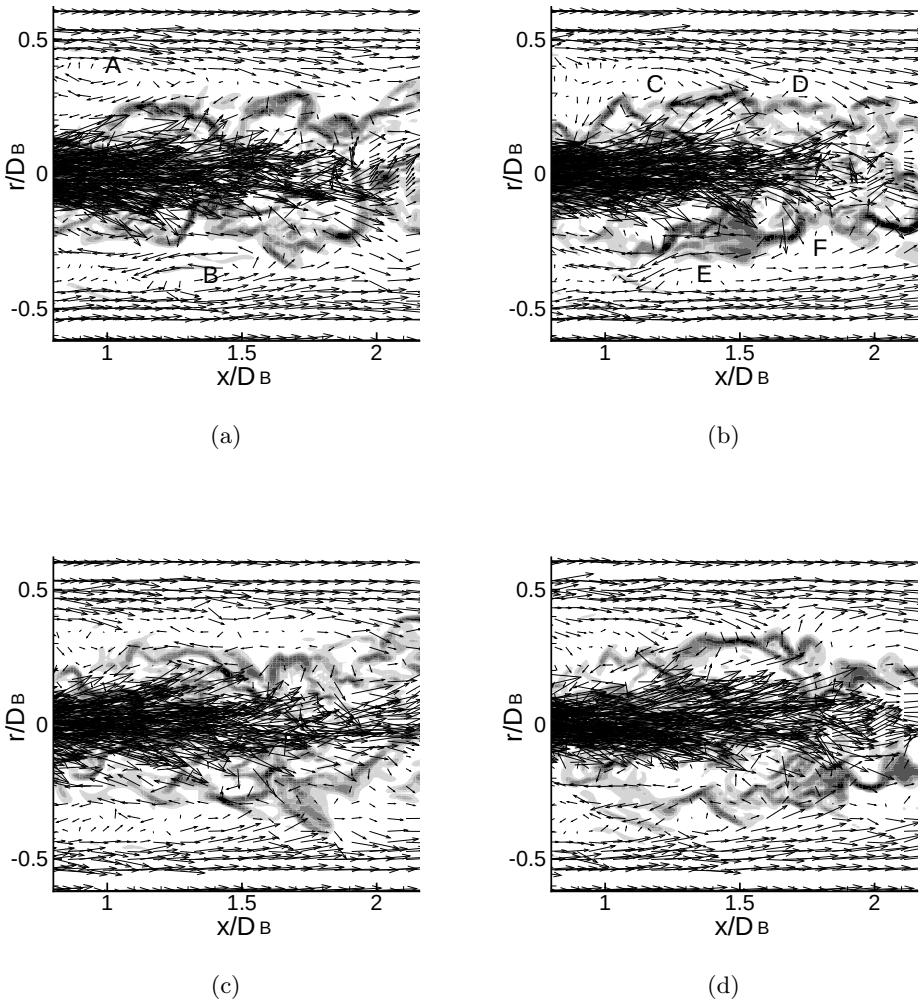

FIGURE 4. Instantaneous fields for the velocity and the scalar dissipation rate (a) t=0 ms (b) t=0.87 ms (c) t=2.5 ms (d) t=3.3 ms.

backward facing step and bluff-body flows (Huerre & Monkewitz 1990; Wee *et al.* 2004). The common ingredient in these flows is the presence of the recirculation zone. The linear stability analysis shows that the velocity profile with the recirculating back flow is absolutely unstable. The dynamics of the present bluff-body flame is more complicated due to the interaction with the main fuel jet. Self-sustained oscillation is observed for both main fuel jet and coflow air streams.

The layer-structure of high scalar dissipation regions is observed in many studies of scalar mixing and jet diffusion flames (Pitsch & Steiner 2000a; Rehm & Clemens 1998; Warhaft 2000). This structure is known to be generated near the hyperbolic point where large scale counter-rotating vortices that carry high and low values of scalars collide with each other (Shriman & Siggia 2000). In their experimental study in plane jet flames,

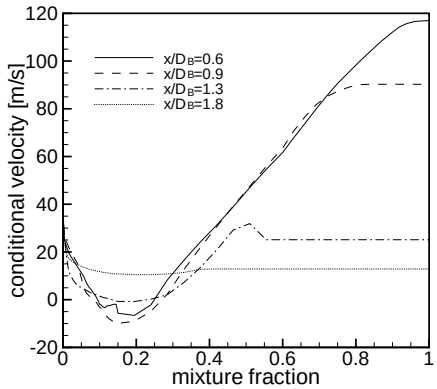

FIGURE 5. Conditional mean velocity.

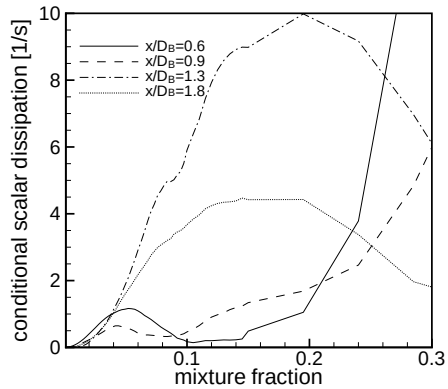

FIGURE 6. Conditional mean scalar dissipation rate.

Rehm & Clemens (1998) observed that the thin OH layer, which is closely associated with a high scalar dissipation layer, is directed inwardly in an angle of approximately 45 degree to the flow direction. This alignment of the high scalar dissipation layers is also observed in LES of jet diffusion flames (Pitsch & Steiner 2000a). This direction corresponds to the normal to the direction of the principal compressive strain in the braid region between two coherent vortical structures of the simple shear flows. On the other hand, high dissipation layers in the intense mixing region of the bluff-body stabilized flame are associated with two additional mechanisms that generate high compressive strain. First, high compressive strain is generated when the high speed main jet stream, which tends to flow outwardly at the end of the recirculating zone, collides with slowly moving outer vortex bubbles, which entrain the air from the coflow stream. Second, high compressive strain is generated near the tip of the expanding high speed main jet. Self-sustained oscillation of the flow structures is responsible for this mechanism. Due to the different origin of high compressive strain, high dissipation layers in the intense mixing region of the bluff-body stabilized flame can be directed inwardly or outwardly in contrast to the simple jet flame. In the present flame, the former is primarily responsible for high dissipation layers on the stoichiometric surfaces, which are of significant importance in the structure of a nonpremixed flame, since the stoichiometric surfaces are primarily located near the outer-side of the recirculation zone.

4.2. *Mixing statistics and flame stabilization*

Figure 5 shows the conditional mean of the axial velocity component at several axial locations. Note that the conditional mean velocity for $0.1 < \eta < 0.25$ is negative at $x/D_B = 0.6$ and 0.9. This range of the mixture fraction corresponds to that in the recirculation zone.

Figure 6 shows the conditional mean scalar dissipation rate at several axial locations. The conditional scalar dissipation rate has two peaks at $x/D_B = 0.6$: one at $\eta \approx 0.05$ and the other at $\eta \approx 0.5$ (not shown). The conditional scalar dissipation rate is very low for $0.1 < \eta < 0.14$ at $x/D_B = 0.6$. This shape of the conditional scalar dissipation is similar to that observed in turbulent piloted jet diffusion flames (Karpetis & Barlow 2002; Pitsch & Steiner 2000b; Kim & Huh 2004). At $x/D_B = 1.3$, significant increase of the conditional scalar dissipation is observed at low values of η. Downstream of $x/D_B = 1.8$,

the conditional scalar dissipation rate at the stoichiometric mixture fraction is similar to that at $x/D_B = 1.3$, while the maximum value decreases significantly. The location of the maximum conditional scalar dissipation rate shifts to a lower value of η.

The recirculation zone of the bluff-body stabilized flame consists of the relatively uniform composition of combustion products, which are primarily generated in the intense mixing region. This helps the flame stabilization in two aspects. First, the scalar dissipation rate on the stoichiometric surfaces is kept low. This is because the stoichiometric scalar dissipation is primarily governed by the mixing between the air in the coflow and the combustion products in the recirculation zone, both of which are abundant at upstream locations. Second, the temperature of combustion products entrained from the intense mixing region is high. These result in a quasi-boundary condition on the slightly rich side, which is favorable to combustion reactions. The present integrated formulation can consider these two aspects of the flame stabilization mechanism. The weighted integral formulation of the conditional velocity allows the entrainment of the combustion products in the neck zone into the recirculation zone. The characteristics of the mixing field observed in the previous section are well represented by the conditional scalar dissipation model, (2.8).

4.3. *Conditional statistics of reactive scalars*

Figure 7 shows conditional means of the temperature and species mass fractions at $x/D_B = 0.6$, 0.9 and 1.8. The temperature and the CO mass fraction are in good agreement with measurements, although the temperature shows slight deviation from measurement on the rich side. NO is over-predicted over the whole range of η. A local minimum of NO at $\eta \approx 0.1$ is observed both in measurements and predictions at $x/D_B = 0.6$. This is because the combustion product entrained by the recirculating flow makes a fairly uniform mixture and prevents direct mixing of fuel and coflow streams. The production of NO is most significant near the stoichiometric mixture fraction where the temperature is highest. The produced NO near the stoichiometric mixture fraction and entrained NO near $\eta \approx 0.13$ do not mix sufficiently due to the low mixing rate at the upstream location of $x/D_B = 0.6$. The overall agreement for the conditional means at $x/D_B = 0.9$ is similar to that at $x/D_B = 0.6$. The prediction still shows a local minimum of NO at this axial location, while this is missing in the measurements. This is because the mixing rate is slightly under-predicted in the recirculation zone. The prediction reproduces the slight decrease of CO and NO at $x/D_B = 1.8$. The decrease of CO and NO is due to high conditional scalar dissipation rate at the stoichiometric mixture fraction at the end of the recirculation zone. This trend is not observed in the previous CMC prediction based on RANS (Kim & Huh 2002).

The accuracy of the predicted conditional statistics is similar to that of the Reynolds averaged CMC (Kim & Huh 2002). NO is not much improved, even with the improved mixing field prediction, while the decrease of NO and CO at the end of the recirculation zone is reproduced here. For sub-filter combustion modeling, the effects of scalar dissipation fluctuations are responsible for this discrepancy. The major part of these is neglected in the present integrated formulation. While the effects of large scale scalar dissipation fluctuations can potentially be considered in the conditional filtering method, the conditional scalar dissipation is averaged over the radial and azimuthal directions in the present formulation. Considering scalar dissipation fluctuations, which induce fluctuations of reactive scalars on the iso-mixture fraction surfaces, the pollutant predictions were shown to be improved (Pitsch 2002; Kim & Huh 2004). Sreedhara & Huh (2005) reported improved prediction of NO and OH for HM1 and HM3 by using second-order

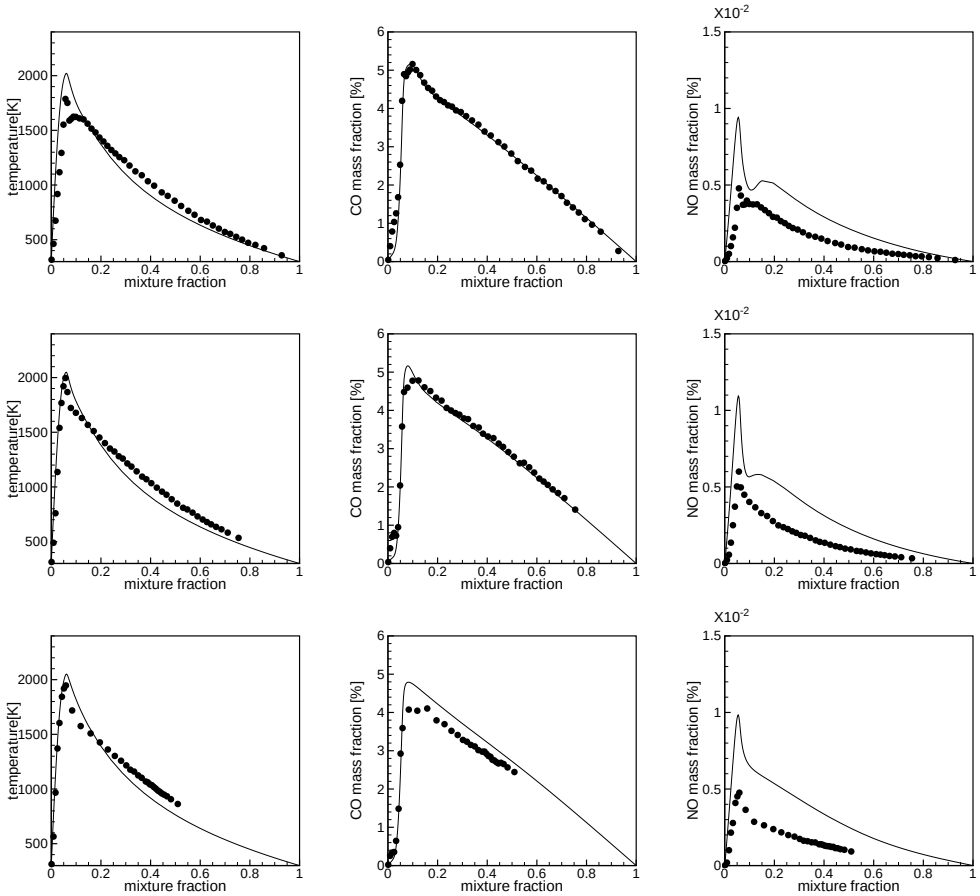

FIGURE 7. Conditional mean temperature and species mass fractions at $x/D_B = 0.6$ (symbols: measurement, lines: prediction)

closure, in which reactive scalar fluctuations on the iso-mixture fraction surfaces are explicitly considered in the evaluation of the reaction rates. However, NO was still over-predicted, even with the second-order CMC, especially for HM1 (Sreedhara & Huh 2005). It is also noted that over-prediction of NO is more pronounced than in piloted jet diffusion flames (Kim & Huh 2004; Roomina & Bilger 2001; Pitsch & Steiner 2000a). Further study is needed to clarify the major source of the observed discrepancy in NO.

The advantage of the present integrated formulation is the significant reduction of the computational cost. The computational time for the integration of the conditionally filtered equations is less than 5% of the overall computation time for the present case. While the integration in two spatial dimensions is performed, the flame structure and NO formation in this complex flame is well represented by the integrated formulation. This makes the present approach attractive to engineering applications.

4.4. *Favre mean statistics of reactive scalars*

Figure 8 shows the radial distributions of temperature and species mass fractions for CO and NO at $x/D_B = 0.9$ and $x/D_B = 1.8$. The predictions are in good agreement with measurement. Overall agreement for the other major species is similar to that in

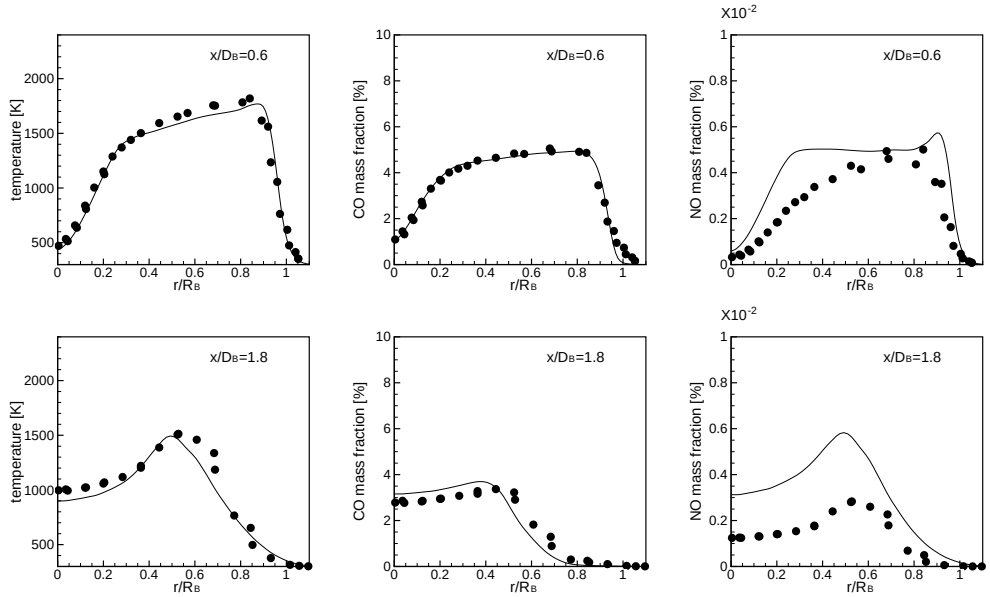

FIGURE 8. Radial distributions of Favre mean temperature and species mass fractions at $x/D_B = 0.6$ and 1.8 (symbols: measurement, lines: prediction)

Fig. 8. The Favre mean statistics of reactive scalars are determined from the statistics of the mixture fraction and the conditionally filtered quantities of reactive scalars. Since there is little local extinction in the present flame, conditionally filtered temperature and species mass fractions are well predicted by the first-order closure of the reaction rate. Accurate prediction of the mixing processes are then of primary importance in the Favre mean field prediction of temperature and mass fractions of major species. The predictions are in good agreement with measured data, while the Favre mean NO mass fraction is over-predicted at $x/D_B = 1.8$. Over-prediction of the Favre mean NO mass fraction is due to the over-predicted conditionally filtered value.

5. Conclusions

Flow dynamics, scalar mixing, and pollutant formation in a turbulent jet diffusion flame stabilized on a bluff-body are investigated using large-eddy simulation. The integrated formulation of the conditional filtering method is presented to consider combustion and pollutant formation at sub-filter scales.

High scalar dissipation is found to occur at the end of the recirculation zone. Vortex shedding from the coflow stream and its interaction with the high speed main jet play an important role in the generation of high dissipation layers in the intense mixing region. Two mechanisms that generate the high dissipation layers are identified. First, high dissipation layers are generated when the high speed main jet stream, which tends to flow outwardly at the end of the recirculating zone, collides with slowly moving outer vortical structures, which entrain the air from the coflow stream. Second, they are generated near the tip of the expanding high speed main jet. Self-sustained oscillations of the flow structures are responsible for this mechanism. In the present flame, the former is primarily responsible for high dissipation layers on the stoichiometric surfaces, which are

of significant importance in the structure of a nonpremixed flame, since the stoichiometric surfaces are primarily located near the outer-side of the recirculation zone.

The characteristics of the flow and mixing fields are well reproduced in the integrated formulation that considers only axial variation of the conditionally filtered quantities. The conditional scalar dissipation in the recirculation zone shows a double peak profile, which is similar to that in a piloted jet diffusion flame. Low scalar dissipation in the recirculated mixture plays a crucial role in the stabilization process. The entrainment of hot combustion products is considered in the weighted integral form of the conditional velocity. The proposed integrated formulation is shown to capture the flame structure and NO formation in this complex flame. The temperature and major species are well predicted, while NO is over-predicted. The decrease of NO and CO at the end of the recirculation zone is reproduced due to a well predicted mixing field. While the use of the cross-section averaged conditional scalar dissipation can be responsible for the over-predicted NO, further study is needed to clarify the major source of the observed discrepancy in NO.

REFERENCES

Brown, P. N., Byrne, G. D., & Hindmarsh, A. C. 1989 VODE: a variable-coefficient ODE solver. *SIAM J. Sci. Stat. Comput.* **10**, 1038-1051.

Dally, B. B., Masri, A. R., Barlow, R. S. & Fiechtner, G. J. 1998 Instantaneous and mean compositional structure of bluff-body stabilized nonpremixed flames. *Combust. Flame.* **114**, 119-148.

Girimaji, S. S. & Zhow, Y. 1996 Analysis and modeling of subgrid scalar mixing using numerical data. *Phys. Fluids.* **8**, 1224-1236.

Herrmann, M., Bulanquart, G. & Raman, V. 2004 Flux corrected finite-volume scheme for preserving scalar boundedness in large-eddy simulations. *Annual Research Briefs 2004*, Center for Turbulence Research, NASA Ames/Stanford Univ.

Huerre, P. & Monkewitz, P. A. 1990 Local and global instabilities in spatially developing flows. *Ann. Rev. Fluid Mech.* **22**, 473-537.

Karpetis, A. N. & Barlow, R. S., 2002 Measurements of scalar dissipation in a turbulent piloted methane/air jet flame. *Proc. Combust. Inst.* **29**, 929-1936.

Kee, R. J., Rupley, F. M. & Miller, J. A 1996 CHEMKIN-II: A Fortran chemical kinetics package for the analysis of gas-phase chemical kinetics, *Report SAND89-8009B*, Sandia National Laboratories.

Kim, S. H. & Huh, K. Y. 2002 Use of the conditional moment closure model to predict NO formation in a turbulent CH_4/H_2 flame over a bluff-body. *Combust. Flame* **130**, 94-111.

Kim, S. H. & Huh, K. Y. 2004 Second-order conditional moment closure modeling of turbulent piloted jet diffusion flames. *Combust. Flame* **138**, 336-352.

Kim, S. H. & Pitsch, H. 2005 Conditional filtering method for large eddy simulation of turbulent nonpremixed combustion. *Phys. Fluids* **17**, 105103.

Klimenko, A. Y. & Bilger, R. W. 1999 Conditional moment closure for turbulent combustion. *Prog. Energy Combust. Sci.* **25**, 595-687.

Liu, K., Pope, S. B. & Caughey, D. A., 2005 Calculations of bluff-body stabilized flames using a joint probability density function model with detailed chemistry. *Combust. Flame* **141**, 153-159.

Lilley, D. K. 1992 A proposed modification of the Germano subgrid-scale closure method. *Phys. Fluids.* **A4**, 633-635.

Masri, A. & Bilger, R. W. 1984 Turbulent diffusion flames of hydrocarbon fuels stabilized on a bluff-body. *Proc. Combust. Inst* **20**, 319-325.

Moin, P., Squires, K., Cabot, W. & Lee, S. 1991 A dynamic subgrid-scale model for compressible turbulence and scalar transport. *Phys. Fluids* **A3**, 2746-2757.

Navarro-Martinez, S., Kronenberg, A. & Mare, F. D. 2005 Conditional moment closure for large eddy simulations. *Flow, Turbu. Combust.* In press.

O'Brien, E. E. & Jiang, T. L., 1991 The conditional dissipation rate of an initially binary scalar in homogeneous turbulence. *Phys. Fluids.* **A3**, 3121-3123.

Pierce, C. D. & Moin, P. 1998 A dynamic model for subgrid-scale variance and dissipation rate of a conserved scalar. *Phys. Fluids.* **10**, 3041-3044.

Pierce, C. D. 1998 Progress variable approach for large-eddy simulation of turbulent combustion. *Ph.D. Thesis*, Stanford University, Stanford CA.

Pitsch, H. & Steiner, H. 2000 Large-eddy simulation of a turbulent piloted methane/air diffusion flame (Sandia flame D). *Phys. Fluids.* **12**, 2541-2554.

Pitsch, H. & Steiner, H. 2000 Scalar mixing and dissipation rate in large-eddy simulations of nonpremixed turbulent combustion. *Proc. Combust. Inst.* **28**, 41-49.

Pitsch, H. 2002 Improved pollutant predictions in large-eddy simulation of turbulent nonpremixed combustion by considering scalar dissipation fluctuations *Proc. Combust. Inst.* **29**, 1971-1978.

Raman, V. & Pitsch, H. 2005 Large eddy simulation of bluff-body stabilized nonpremixed flame using a recursive refinement procedure. *Combust. Flame.* **142**, 329-347.

Rehm, J. E. & Clemens, N. T. 1998 The relationship between vorticity/strain and reaction zone structure in turbulent non-premixed jet flames. *Proc. Combust. Inst.* **27**, 1113-1120.

Roomina, M. R. & Bilger, R. W., 2001 Conditional moment closure (CMC) predictions of a turbulent methane-air jet flame. *Combust. Flame.* **125**, 1176-1195.

Shriman, B. I. & Siggia, E. D. 2000 Scalar turbulence. *Nature* **405**, 639-646.

Sreedhara, S. & Huh, K. Y. 2005 Modeling of turbulent, two-dimensional nonpremixed CH4/H2 flame over a bluff-body using first- and second-order elliptic conditional moment closures *Combust. Flame.* **143**, 119-134.

Sung, C. J., Law, C. K. & Chen, J.-Y. 2001 Augmented reduced mechanisms for NO emission in methane oxidation. *Combust. Flame.* **125**, 906-919.

Tang, Q., Xu, J. & Pope, S. B. 2000 Probability density function calculations of local extinction and NO production in piloted jet turbulent methane/air flames. *Proc. Combust. Inst.* **29**, 133-139.

Warhaft, Z. 2000 Passive scalars in turbulent flows. *Ann. Rev. Fluid Mech.* **32**, 203-240.

Wee, D., Yi, T., Annaswamy, A. & Ghoniem, A. F., 2004 Self-sustained oscillations and vortex shedding in backward-facing step flows: Simulation and linear instability analysis. *Phys. Fluids.* **16**, 3361-3373.